

# PointDreamer: Zero-shot 3D Textured Mesh Reconstruction from Colored Point Cloud

Qiao Yu, Xianzhi Li✉, Yuan Tang, Xu Han, Jinfeng Xu, Long Hu, and Min Chen, *Fellow, IEEE*

**Abstract**—Reconstructing textured meshes from colored point clouds is an important but challenging task. Most existing methods yield blurry-looking textures or rely on 3D training data that are hard to acquire. Regarding this, we propose PointDreamer, a novel framework for textured mesh reconstruction from colored point cloud via diffusion-based 2D inpainting. Specifically, we first reconstruct an untextured mesh. Next, we project the input point cloud into 2D space to generate sparse multi-view images, and then inpaint empty pixels utilizing a pre-trained 2D diffusion model. After that, we unproject the colors of the inpainted dense images onto the untextured mesh, thus obtaining the final textured mesh. This project-inpaint-unproject pipeline bridges the gap between 3D point clouds and 2D diffusion models for the first time. Thanks to the powerful 2D diffusion model pre-trained on extensive 2D data, PointDreamer reconstructs clear, high-quality textures with high robustness to sparse or noisy input. Also, it’s zero-shot requiring no extra training. In addition, we design Non-Border-First unprojection strategy to address the border-area inconsistency issue, which is less explored but commonly-occurred in methods that generate 3D textures from multiview images. Extensive qualitative and quantitative experiments on various synthetic and real-scanned datasets show the SoTA performance of PointDreamer, by significantly outperforming baseline methods with 30% improvement in LPIPS score (from 0.118 to 0.068). Code at: <https://github.com/YuQiao0303/PointDreamer>.

**Index Terms**—Point Cloud Reconstruction, Texture Mapping, 2D Diffusion, Image Inpainting.



This work has been submitted to the IEEE for possible publication. Copyright may be transferred without notice, after which this version may no longer be accessible.

## 1 INTRODUCTION

3D point clouds and meshes are two of the most fundamental 3D modalities in computer vision, graphics, and robotics. Reconstructing 3D textured meshes from colored point clouds (*abbr.* colored-PC-to-mesh) is a pivotal task, with extensive applications like digital twin [1], meta-verse [2], cultural heritage preservation [3], etc. It requires the accurate reconstruction of both geometry and colors, to transform sparse and unstructured data into coherent and visually appealing models.

While recent methods [4]–[6] have achieved relatively satisfactory geometry reconstruction quality, color reconstruction remains challenging, especially for low-density point clouds. Unlike images that provide dense pixel-level representations, the inherent sparse nature of point clouds makes it difficult to reconstruct dense colors. Regarding this, existing methods either blend input points’ colors by interpolation [7] or overfitting [8], [9], or train color prediction networks [10], [11] with 3D datasets. However, they often

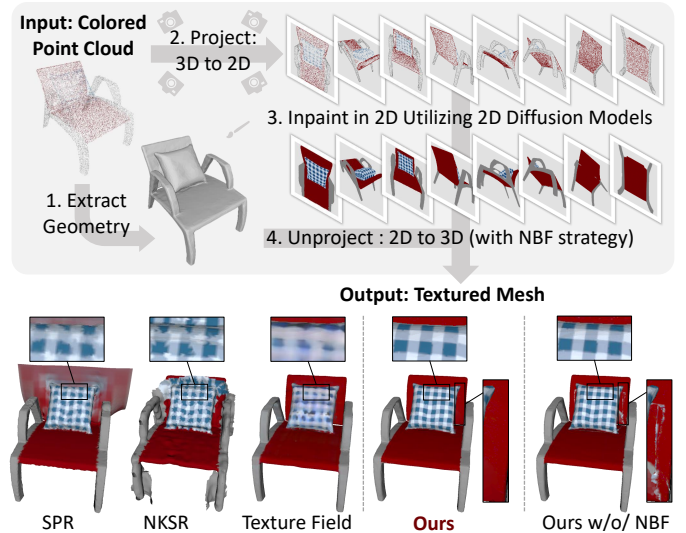


Fig. 1. PointDreamer is a zero-shot framework to reconstruct 3D textured meshes from colored point clouds. It produces textures with higher quality compared to baseline methods. Its specially designed NBF unprojection strategy effectively addresses the border-area artifact issue.

yield blurring-looking textures; see SPR [7], NKSR [9], and Texture Field [10], [12] in Figure 1. Also, 3D training data are notoriously challenging to acquire.

While the colored-PC-to-mesh task remains challenging, 2D image generation has recently thrived with impressive plausibility, level of detail, and generalization capability. Therefore, many works [13], [14] leverage 2D diffusion models for 3D generation. Since the scale of existing 2D datasets

- Qiao Yu, Xianzhi Li, Yuan Tang, Xu Han, Jinfeng Xu are with Huazhong University of Science and Technology, Wuhan, China, E-mail: {qiaoyu\_epic, xzli, yuantang, xhanxu, jinfengxu}@hust.edu.cn.
- Long Hu is with Guangdong HUST Industrial Technology Research Institute and also with School of Computer Science and Technology, Huazhong University of Science and Technology, Email: longhu@hust.edu.cn.
- Min Chen is with the School of Computer Science and Engineering, South China University of Technology, Guangzhou, China, and also with the Pazhou Laboratory, Guangzhou, China, E-mail: minchen@ieee.org. Corresponding author: Xianzhi Li

far exceeds that of 3D datasets, leveraging diffusion models pre-trained on extensive 2D datasets can also significantly alleviate the reliance on 3D datasets. This inspires us to adopt 2D diffusion models for the colored-PC-to-mesh task, to address the low-quality color reconstruction issue.

However, it is not trivial to implement this idea: **(1)** Existing 2D-diffusion-for-3D methods typically focus on 3D generation conditioned on text [15], [16] or images [17], [18], leaving point-cloud-based reconstruction unexplored. **(2)** Existing 2D-diffusion-for-3D methods often yield blurry appearances [19] by predicting colors in 3D space as a texture [16], [20]/radiance [21]–[23] field or 3D Gaussians [18], [19]. How to leverage 2D reference images to generate high-quality textures requires more attention. **(3)** Intermediate 2D multiview images generated by diffusion models often have inconsistencies with each other or with the reconstructed 3D geometry at occlusion border areas. When one part of an object occludes another, the generated 2D images and 3D geometry should predict highly consistent occlusion borders. Failing to do so would cause artifacts; see “Ours w/o NBF” in Figure 1, with significant artifacts near the border of the pillow and the chair.

We address these challenges one by one. **First**, to bridge the gap between 2D diffusion models and 3D point clouds, our intuition is that, reconstructing 3D textured meshes from colored point clouds is analogous to inpainting 2D sparse images by filling empty pixels. They both aim to somehow *dreaming* the missing areas of the sparse input, to achieve a more complete and coherent representation. Luckily, 2D diffusion-based inpainting methods [24] excel even with mask ratios over 80%, making them robust to sparse input points. Trained on large-scale 2D datasets, these models generalize well across domains and require no additional training or fine-tuning, enabling zero-shot point cloud reconstruction. **Second**, to address the blurring issue, we propose to directly unproject the generated multiview images onto the 3D mesh, instead of predicting colors in 3D [9], [10] or UV [8] spaces like existing methods. **Third**, to address the occlusion-border inconsistency issue, we design a “Non-Border-First” (NBF) unprojection strategy. It detected border areas by leveraging the correspondence of occlusion border in 2D image space and invisibility border in UV space, and then prioritizes non-border views’ images during unprojection, thus avoiding artifacts.

Putting everything together, we propose *PointDreamer*, a novel zero-shot framework to reconstruct high-quality textured meshes from colored point clouds, as shown in Figure 1. First, we extract geometry (untextured mesh) from the point cloud by an existing method POCO [4]. Second, we project the point cloud into 2D space from a fixed set of viewpoints, producing multiview sparse images. Third, we inpaint the empty pixels with an off-the-shelf 2D diffusion model, forming dense images. Finally, we directly unproject the 2D images onto the mesh. Unlike most existing methods that predict colors in 3D [10], [11] or UV spaces [8], directly adopting colors of 2D diffusion models’ output high-quality 2D images leads to clear textures. In particular, our designed NBF unprojection strategy effectively avoids artifacts caused by inconsistencies in occlusion border regions.

Overall, we list our contributions below:

- We propose *PointDreamer*, a zero-shot SoTA framework that fills the gap in the less-explored but important task of 3D textured mesh reconstruction from colored point cloud, pioneering in utilizing 2D diffusion models for 3D point cloud reconstruction.
- *PointDreamer* reconstructs high-quality and clear-looking textures for meshes, avoiding the common blurring issue. *PointDreamer* is also zero-shot. While requiring no extra training, it shows high generalization capability: robust to noisy, sparse, or even incomplete input points, benefiting from the power of 2D diffusion models.
- We design Non-Border-First (NBF) Unprojection, a novel unprojection strategy to apply colors of 2D multiview images onto 3D meshes. It effectively avoids artifacts caused by inconsistent prediction near occlusion borders in any multiview-images-to-3D methods.

Experiments on various benchmarks show the **SoTA** performance of *PointDreamer*, by significantly outperforming baseline methods quantitatively and qualitatively.

## 2 RELATED WORK

### 2.1 Textured Mesh Reconstruction from Colored Point Cloud

Existing methods can be categorized based on their reliance on training data. **Non-data-driven** methods rely solely on the input point cloud. For instance, (Screened) Poisson Surface Reconstruction (PSR, SPSR) [7], [25] reconstructs geometry by solving Poisson equations, and many 3D processing tools [26], [27] extend it with color support via linearly blending input point colors. DHSP3D [8] iteratively optimizes a MeshCNN in 3D space and XYZ/RGB maps in UV space by self-supervision. On the other hand, **data-driven** methods train neural networks on 3D datasets to generate textured meshes. For example, 3DGen [10] trains a triplane variational autoencoder to predict signed distance field and color values for each 3D tetrahedra grid vertex, and extracts textured meshes by marching tetrahedra [28]. **Hybrid** methods employ different strategies for geometry and texture reconstruction. NKSR [9] adopts data-driven geometry reconstruction by learning neural kernel fields, while using non-data-driven color reconstruction (in its supplementary file), by optimizing a 3D textured field [12] to overfit the input points’ colors. ColorMesh [11] employs non-data-driven geometry reconstruction via graph cuts, paired with a data-driven texture network to inpaint colors in 2D image space. However, its texture network is an encoder-decoder CNN trained with limited data. This may limit its performance and generalization capability, compared to our adopted zero-shot 2D-diffusion-based inpainting approach trained with extensive 2D data.

### 2.2 2D Diffusion Models for 3D Generation

To capitalize on the abundant availability of 2D data and the high performance of 2D diffusion models, researchers seek to “lift” results of 2D diffusion models to 3D. Most of these works optimize or learn a NeRF [22], [23], a DM Tet with texture field [16], [29], or 3D Gaussians by Score

Distillation Sampling [13] or reconstruction loss to make the generated 3D scene similar to the result of a given 2D diffusion model. View-conditioned diffusion models [22] or multi-view diffusion models [14], [30], [31] are developed by fine-tuning existing diffusion models for generating multi-view-consistent images. Most of these works focus on 3D generation from text or images instead of point clouds. They tend to generate blurry textures, and may suffer from artifacts in occlusion border areas.

### 2.3 Border-Area-Inconsistency Issue in 3D Texturing

Mesh texture reconstruction based on real-scanned or AI-generated multiview images is widely used in applications such as 3D reconstruction and generation [32]. Due to scanning errors and imperfections in generative models, inconsistencies often arise between different views’ images or between images and the mesh, especially around occlusion borders where one part of the object occludes another. However, this issue remains largely unexplored. Most texture mapping methods [33]–[36] design complex optimization objectives and strategies for camera extrinsics, etc. They typically focus on issues like blurring, ghosting, and seams, leaving border-area-inconsistency unexplored. Also, they predominantly rely on RGBD data, and thus are unsuitable for scenarios without dense depth data like point cloud reconstruction. On the other hand, most 3D generation approaches directly fuse multiview images’ colors for mesh texturing. Specifically, they use these images as supervision during optimization [32], or directly compute image colors’ weighted sum as the mesh’s colors [37]. To address the border-area-inconsistency issue, we design a Non-Border-First unprojection strategy, and it can be used in any method that unprojects multiview images to a mesh.

## 3 METHOD

Given a 3D point cloud with per-point XYZ coordinates and RGB colors, our goal is to reconstruct its associated textured mesh. To avoid the blurring effect of existing works, we predict colors in 2D space by diffusion-based 2D inpainting, leveraging the powerful 2D diffusion priors. Figure 1 presents our designed pipeline with four steps. (1) We employ a geometry extraction module to reconstruct an untextured mesh from the input point cloud. (2) With a set of fixed viewpoints, we perform 3D-to-2D conversion by projecting the input point cloud into 2D, producing sparse multi-view images. (3) We conduct color prediction in 2D space by inpainting the empty pixels in the sparse images to form dense ones based on a pre-trained 2D diffusion model [38]. (4) We propose a novel Non-Border-First strategy to convert the 2D results back to 3D by unprojecting the colors in the dense images to the untextured mesh to produce the desired textured mesh.

Note that with the 2D diffusion priors, our method is zero-shot requiring no extra training. It takes only about 61s and 30s for PointDreamer’s DDNM and nearest/linear interpolation variants (see Figure 7 (b)) to reconstruct a shape of 30k points on an NVIDIA A100 GPU, compared to other 2D-diffusion-for-3D methods such as Zero-1-to-3 [22] (~20 m), DreamGaussin [19] (~2 m), Wonder3D [32] (2~3 m), LGM [18] (~65 s), etc.

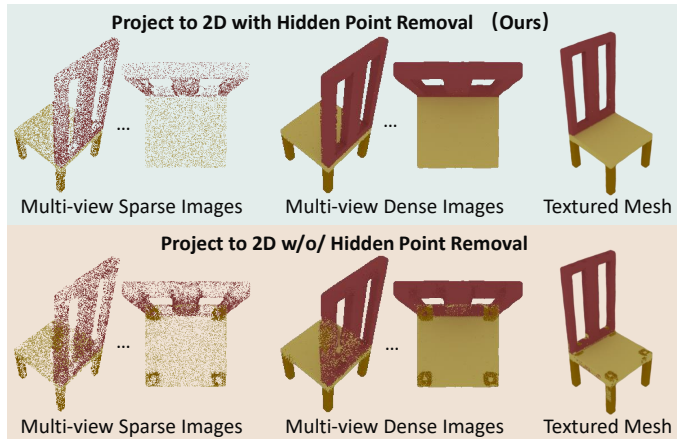


Fig. 2. Illustration of hidden point removal, without which the results would be messed up.

### 3.1 Geometry Extraction: Point to Surface

The first step in PointDreamer is to reconstruct an untextured mesh from the input point cloud. Since color information does not need to be considered in this step, many existing point-to-surface methods [28], [39], [40] can be employed. In our implementation, we directly adopt the state-of-the-art POCO<sup>1</sup> [4] for its high performance. We conduct experiments comparing different geometry reconstruction methods in Section 4 and our supplementary file.

### 3.2 Projection: 3D to 2D

Directly projecting the whole point cloud into 2D space would incorporate points from occluded parts that should not be visible from the given view. This would mess up the inpainting results and subsequent mesh textures; see Figure 2 for an example. Therefore, before generating the sparse images, we process the input point cloud by the “Hidden Point Removal” operator [41], which works by transforming the input and extracting the points that reside on its convex hull. Besides, we compare the depth values of points and the extracted untextured mesh to further remove some invisible points. With pre-set camera parameters of  $K$  viewpoints ( $K = 8$  in our implementation) and associated visible point clouds, we conduct camera transformation to these points to get their corresponding pixel coordinates in 2D image space. These pixels are painted according to their associated 3D points’ colors, producing  $K$  sparse images. **We compare different  $K$  values in our supplementary file.**

### 3.3 Inpainting: Sparse to Dense

Any 2D inpainting method that fills empty pixels in input images can serve as our inpainting module. We propose to use the state-of-the-art DDNM<sup>2</sup> [24] based on a pre-trained unconditional 2D diffusion model<sup>3</sup> [38] to inpaint the multi-view sparse images into dense ones  $\mathbf{I} = \{I_k\}_{k=1}^K$ . In this way, the 2D diffusion model’s strong prior can facilitate high-quality inpainting. So far, we have completed color prediction purely in 2D space instead of 3D or UV space.

1. <https://github.com/valeoai/POCO>

2. <https://github.com/wyhuai/DDNM>

3. <https://github.com/openai/guided-diffusion>

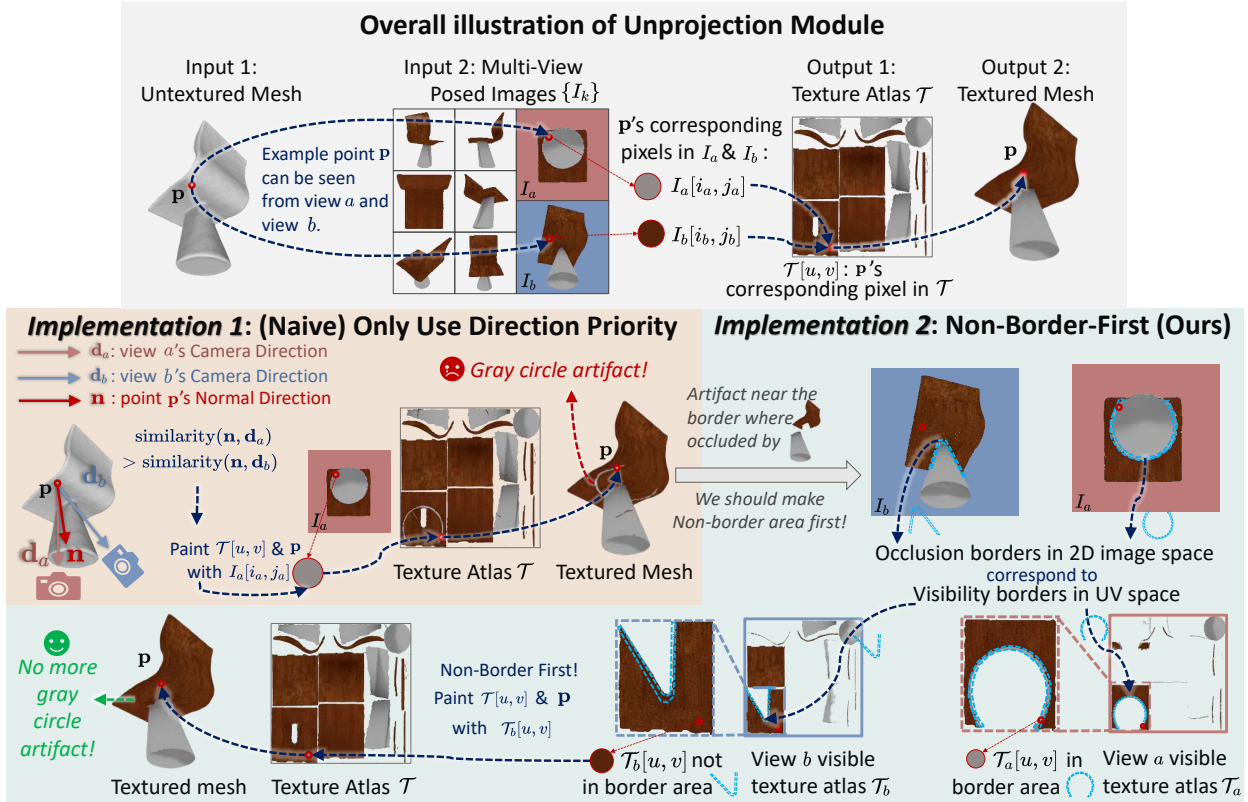


Fig. 3. *Top*: Illustration of input and output of the unprojection module, which unprojects colors of 2D multi-view images to a 3D mesh. *Middle Left*: An naive unprojection implementation. For each 3D point  $p$ , from all views where  $p$  is visible, the highest-direction-priority view is chosen to paint  $p$ . Example point  $p$ 's corresponding pixel in the selected view  $a$  is with incorrect color since it's near an occlusion border, producing an artifact. *Bottom Right*: our proposed Non-Border-First Unprojection. Observing the correspondence between the occlusion border in 2D image space and the visibility border in UV space (both marked by sky-blue dashed lines), we prioritize non-border areas in UV space to avoid such artifacts.

### 3.4 Unprojection: 2D to 3D

With color prediction conducted in 2D space, we now need to convert the result back to 3D. Specifically, the goal is to use the extracted untextured mesh and inpainted multi-view posed images, to generate the associated textured mesh. Regarding this, we design a novel approach namely "Non-Border-First Unprojection".

The top of Figure 3 illustrates the basic idea of the unprojection module. Specifically, we represent mesh texture as a texture atlas  $\mathcal{T}$  by applying UV mapping to a mesh  $\mathcal{M}$ . We follow existing works [32], [42] to conduct UV mapping by Xatlas [43]. A texture atlas is an RGB image containing different charts. Each chart is a continuous area in UV space that corresponds to a continuous segment of  $\mathcal{M}$  in 3D space. Each pixel  $\mathcal{T}[u, v]$  of a chart corresponds to a surface point  $p$  of  $\mathcal{M}$ . Therefore, our goal is to assign a color for each chart pixel  $\mathcal{T}[u, v]$ . Given a set of multi-view posed images  $\mathbf{I} = \{I_k\}_{k=1}^K$ ,  $p$  can be seen in zero, one, or more images. If  $p$  is visible in  $I_k$ , we denote  $I_k$ 's corresponding pixel as  $I_k[i_k, j_k]$ . See the top of Figure 3 as an example, where a 3D point  $p$  is visible in two views  $a$  and  $b$ , and we mark it with a red circle together with its corresponding multi-view image pixels  $I_a[i_a, j_a]$ ,  $I_b[i_b, j_b]$ , and texture atlas pixel  $\mathcal{T}[u, v]$ .

Point  $p$ 's visibility in view  $k$  can be calculated by whether its depth value is no bigger than the corresponding pixel of the  $k$ 's depth map. If  $p$  is visible only in one view, the corresponding color of  $I_k[i_k, j_k]$  can be directly

adopted as the color of  $p$  and  $\mathcal{T}[u, v]$ . If  $p$  can be seen in no view at all, we can set some rules to deal with it. If  $p$  can be seen in more than one view, we can try to fuse the corresponding colors or select one best view. Various unprojection strategies differ in how to fuse views or select the best view. Here we introduce three different implementations for unprojection.

#### 3.4.1 Naive Unprojection: Only Use Direction Priority

An intuitive idea to pick the best view for  $p$  or  $\mathcal{T}[u, v]$  is by direction priority, as shown in the middle left part of Figure 3. Specifically, for each view  $k$  where point  $p$  can be seen, we calculate the direction priority score  $s_p(k)$ , defined as the cosine similarity of  $p$ 's normal direction  $n$  and view  $k$ 's camera direction  $d_k$ . The view with the highest direction priority is chosen to paint  $p$  and  $\mathcal{T}[u, v]$ . For example, in the middle left part of Figure 3,  $p$  is painted to gray according to  $I_a[i_a, j_a]$  since view  $a$  has a higher direction priority. Also, if there are a few points invisible from any view, we can still assign a view by direction priority.

While this naive unprojection strategy serves adequately for most points, it produces artifacts under certain circumstances; see again the middle left part of Figure 3, where a gray artifact is visible in the reconstructed textured mesh that should have been brown. Through analysis, such artifacts appear in *border areas*: the area near the border of occluded and occluding part of the shape when viewing from view  $k$ . For example, in view  $a$ , the brown seat's

**Algorithm 1** PyTorch-like pseudocode for Non-Border-First (NBF) strategy

---

```

1 # K: number of views
2 # T: texture atlas
3 # I: multiview images
4 # I_dep: [K, I_res, I_res], multi-view depth maps obtained from geometry
5 # T_dep: [K, T_res, T_res], T's pixels' corresponding depths in each view
6 # Tuv2Iab: [T_res, T_res, 2]: Mapping T's pixel coordinate to I's
7 # chart_mask: [T_res, T_res]: Does T(u,v) belong to a chart (in foreground)?
8 # T_normal: [T_res, T_res, 3]: T's pixels' corresponding 3D point' normal directions
9 # view_dir: [K, 3]: camera view directions
10 # I_rgb: [K, I_res, I_res, 3], multi-view RGB images
11 T = torch.zeros(T_res, T_res, 3)
12 vis_T = calc_vis(I_dep, T_dep, Tuv2Iab) # [K, T_res, T_res], bool
13 vis_T_edges = detect_edge(vis_T) # [K, T_res, T_res], bool
14 chart_edges = detect_edge(chart_mask) # [T_res, T_res], bool
15 border_edges = vis_T_edges - chart_edges.unsqueeze(0).repeat(K)
16 border_areas = dilate(border_edges, kernel) # [K, T_res, T_res], bool
17 cand_view_T_map = non_border_areas = ~border_areas # [K, T_res, T_res]
18 Tuv_cand_view_num = non_border_areas.sum(0) # [T_res, T_res], int
19 cand_view_T_map[:, Tuv_cand_view_num==0] = vis_T[:, Tuv_cand_view_num==0]
20 dir_priority = calc_priority(T_normal, view_dir) # [K, T_res, T_res]
21 dir_priority[~cand_view_T_map] -= 1000 # Non-Border-First
22 uv_view_id = dir_priority.argmax(0) # [T_res, T_res]
23 for u in range(0, T_res):
24     for v in range(0, T_res):
25         T[u, v] = I_rgb[uv_view_id[u, v], Tuv2Iab[u, v, 0], Tuv2Iab[u, v, 1]]

```

---

bottom side is occluded by the gray bottom of the chair. The area near the edge of the brown and gray parts is a border area. In such areas, the inpainting module and the geometry extraction module may inconsistently delineate the boundary separating the two parts. For example, the gray bottom is larger in the inpainted image  $I_a$  than of the reconstructed mesh, thus resulting in an artifact.

### 3.4.2 Optimization-based Unprojection

Instead of selecting one single view by direction priority, 3D generation method DreamGaussian [19] adopts an optimization-based strategy to get the textured mesh from multi-view images. The idea is to optimize the texture atlas by a per-pixel loss between the inpainted multi-view images  $\{I_k\}_{k=1}^K$  and the rendered images of the reconstructed textured mesh. In this way, the optimization process kinds of *fuses* corresponding colors in different views instead of selecting the best one. However, it cannot ignore the inconsistent colors in the *border areas*, so the artifacts can only be reduced instead of eliminated. This inspires us to design a non-border-first strategy to address this issue.

### 3.4.3 Non-Border-First Unprojection (NBF)

The bottom of Figure 3 illustrates the idea of our proposed novel unprojection strategy namely Non-Border-First Unprojection. It begins with detecting *border areas* in multi-view images, so as to paint the texture atlas while deprioritizing them. After that, if some atlas pixels remain unpainted since their associated 3D points can not be seen from any non-border area, we then select from all areas, whether they are border areas or not, to paint the rest pixels. Now the question is, how to accurately detect *border areas*.

Interestingly, we find that, the borders between occluded and occluding parts of the shape in image  $I_k$  (2D space) often correspond to the borders between visible and invisible areas in “view  $k$  visible texture atlas  $\mathcal{T}_k$ ” (UV space), where  $\mathcal{T}_k$  is defined as a texture atlas in which only visible areas in view  $k$  are filled and rest invisible areas are empty.

See the bottom of Figure 3 as an example, where such border areas are marked by sky blue dashed lines. In posed images  $I_a$  and  $I_b$ , these areas divide the occluded brown seat and the occluding gray bottom, while in view  $a$  and  $b$  visible texture atlas  $\mathcal{T}_a$  and  $\mathcal{T}_b$ , these areas divide the visible (painted) and invisible (transparent) parts in view  $a$  and  $b$ , respectively. The reason for this correspondence of UV visibility border and 2D occlusion border is that, a continuous area within a chart of the texture atlas usually corresponds to a continuous segment of the 3D surface. When a chart contains both visible and invisible regions in a given view  $k$ , it often indicates that the corresponding 3D areas of invisible regions are occluded by some other part of the shape. Therefore, we design our Non-Border-First unprojection strategy as follows.

- 1) We paint “view  $k$  visible texture atlas map”  $\mathcal{T}_k$  for each view  $k$  defined as above.
- 2) We calculate the border areas by dilating the edges between visible and invisible areas in  $\mathcal{T}_k$  given a certain dilation kernel size as a hyperparameter.
- 3) We paint the final texture atlas  $\mathcal{T}$  considering only non-border areas in  $\mathcal{T}_k$ . During this, if a point is visible in more than one view’s non-border areas, we select the view with the highest direction priority.
- 4) If there remain some unpainted pixels in  $\mathcal{T}$ , check the previously ignored border areas to paint them, during which we still select among views by direction priority.
- 5) If some points cannot be seen from either view, we assign it with a view by direction priority considering all areas in all views whether they’re border areas or not.
- 6) We experimentally find that additionally optimizing from the generated texture atlas by only calculating the loss of non-border pixels would further enhance the results.

In this way, our non-border-first strategy can reason-

ably eliminate artifacts caused by inconsistent prediction in border areas. Algorithm 1 shows the corresponding pseudoCode. We conduct experiments to verify the effectiveness of our proposed strategy in Section 4.

## 4 EXPERIMENTS AND RESULTS

### 4.1 Experimental Settings

#### 4.1.1 Datasets

To evaluate the performance of our method against other competitors, we use three benchmark datasets:

(i) **ShapeNetCoreV2** [44]: A large-scale synthesis 3D object dataset, where we follow [42] to use the official test splits of *chair*, *car*, and *motorbike* categories for evaluation, since they contain relatively complex textures. The test sets of the three categories contain around 1300, 690, and 70 samples, respectively.

(ii) **Google Scanned Objects (GSO)** [45]: A real-scanned 3D object dataset and we use all its 1030 samples for evaluation, unlike existing works [14], [32] that only use 30 of them.

(iii) **OmniObject3D** [46]: A real-scanned 3D object dataset with 6000 samples. For efficiency, we randomly select 100 objects for evaluation.

For each textured mesh from the above datasets, we sample 30k colored points as input. Note that, our approach is zero-shot and can be directly applied to objects from various datasets or categories, requiring no extra training but only an off-the-shelf 2D diffusion model [38].

#### 4.1.2 Metrics

To evaluate the quality of the reconstructed 3D textured mesh, we follow existing works [14], [22], [32], [47] to compare the similarity between multi-view images rendered by the reconstructed mesh and ground-truth mesh. Specifically, we render 20 images per shape for a thorough assessment by distributing cameras on the vertices of a regular icosahedron. Four similarity metrics are calculated: Peak Signal-to-Noise Ratio (PSNR), Structural Similarity Index Measure (SSIM) [48], Learned Perceptual Image Patch Similarity (LPIPS) [49], and Fréchet Inception Distance (FID) [50]. PSNR and SSIM focus more on pixel-level similarity, while LPIPS and FID imitate human perception better. Since we focus on texture instead of geometry reconstruction, **we put geometry evaluation results in our supplementary file.**

### 4.2 Baselines

To fully evaluate the performance of our method, we compare it with three kinds of baseline methods:

(1) **Screened Poisson Reconstruction (SPR)** [7]: SPR is a classical mesh reconstruction method. We adopt the implementation of the commonly-used tool MeshLab [26], which generates texture by linearly blending colors of the input point cloud. Note that SPR requires per-point normal as input, which we estimate via MeshLab’s default Principal Component Analysis (PCA).

(2) **DHSP3D** [8] and **NKSR** [9]: These are two recent approaches for mesh reconstruction which generate textures by overfitting the input points’ colors. We employ the official



Fig. 4. Qualitative results on (a) ShapeNetCoreV2 dataset (Chair, Car, Motorbike Category), (b) GSO dataset, (c) OmniObject3D dataset. (d) Comparison with DHSP on GSO. (e) Our Multiview Consistency.

code provided by the authors<sup>4</sup>. Similar to SPR, NKSR also requires point normals as additional input.

(3) **Texture Field (T.F.)** [12]: Since we cannot find any existing open-source texture-field-based method requiring only colored point clouds as input, we thus design a baseline network inspired by [10]. The key idea is to learn a 3D feature tri-plane from the input point cloud and then decode RGB values for the query points. We train it on the official training split of the mentioned three categories of ShapeNetCoreV2, supervised by per-point color MSE loss following [10]. During inference, we employ the above-mentioned POCO [4] to reconstruct untextured meshes. Then we utilize our trained T.F. network to infer textures, by querying colors for the associated 3D point of each texture atlas pixel. In this way, both PointDreamer and the T.F. baseline adopt the same geometry module for a fair

4. <https://github.com/weixk2015/DHSP3D>,  
[https://github.com/nv-tlabs/NKSR/blob/public/examples/recons\\_colored\\_mesh.py](https://github.com/nv-tlabs/NKSR/blob/public/examples/recons_colored_mesh.py)

TABLE 1

Comparisons on textured mesh reconstruction on ShapeNetCoreV2, GSO and Omniobject3D datasets. T.F. refers to Texture Field. Note that both T.F. and our PointDreamer adopt POCO [4] for geometry reconstruction for a fair comparison.

| ShapeNet Cat. | Method | PSNR $\uparrow$ | SSIM $\uparrow$ | LPIPS $\downarrow$ | FID $\downarrow$ |
|---------------|--------|-----------------|-----------------|--------------------|------------------|
| Chairs        | SPR    | 24.10           | 0.931           | 0.092              | 12.03            |
|               | NKSR   | 23.05           | 0.931           | 0.096              | 29.11            |
|               | T.F.   | 26.12           | 0.947           | 0.066              | 6.83             |
|               | Ours   | <b>26.29</b>    | <b>0.952</b>    | <b>0.057</b>       | <b>4.90</b>      |
|               |        |                 |                 |                    |                  |
| Cars          | SPR    | <b>23.46</b>    | 0.929           | 0.088              | 43.89            |
|               | NKSR   | 21.01           | 0.919           | 0.096              | 131.05           |
|               | T.F.   | 22.42           | 0.919           | 0.087              | 38.08            |
|               | Ours   | 22.78           | <b>0.930</b>    | <b>0.073</b>       | <b>12.41</b>     |
| Motorbikes    | SPR    | 15.09           | 0.809           | 0.214              | 106.09           |
|               | NKSR   | 18.13           | 0.905           | 0.101              | 175.42           |
|               | T.F.   | 21.17           | 0.926           | 0.064              | 40.06            |
|               | Ours   | <b>21.20</b>    | <b>0.930</b>    | <b>0.056</b>       | <b>28.42</b>     |
|               |        |                 |                 |                    |                  |
| Dataset       | Method | PSNR $\uparrow$ | SSIM $\uparrow$ | LPIPS $\downarrow$ | FID $\downarrow$ |
| GSO           | SPR    | 27.11           | 0.907           | 0.120              | 27.43            |
|               | NKSR   | 24.65           | 0.900           | 0.118              | 36.51            |
|               | T.F.   | 25.53           | 0.894           | 0.128              | 46.44            |
|               | Ours   | <b>27.24</b>    | <b>0.923</b>    | <b>0.083</b>       | <b>9.32</b>      |
| OmniObject3D  | SPR    | <b>30.20</b>    | 0.927           | 0.100              | 40.13            |
|               | NKSR   | 26.77           | 0.919           | 0.105              | 50.14            |
|               | T.F.   | 28.08           | 0.914           | 0.112              | 65.61            |
|               | Ours   | 29.78           | <b>0.941</b>    | <b>0.068</b>       | <b>18.23</b>     |

comparison. Please refer to our supplementary file for more details about the training and inference of our T.F. baseline.

## 4.3 Main Results

### 4.3.1 Qualitative Results

We present visual results in Figure 4. Since DHSP3D is much slower than other methods (4-6 hours per shape compared to <1 min), we randomly select two objects from GSO dataset for efficiency during comparison. **We highly recommend referring to our supplementary materials for more visual results and a 360° video.**

Figure 4 (a)-(d) show that our method, though zero-shot, achieves much clearer and more realistic textures than baselines, thanks to the 2D diffusion prior. Besides, SPR and NKSR, which both rely on per-point normals as input, sometimes yield redundant geometry mainly due to the wrongly-estimated normal direction. The texture field baseline, which is trained on ShapeNetCoreV2, performs much worse on the newly-seen dataset of GSO and Omniobject3D, indicating a lack of generalization ability. In Figure 4 (d), the red cup in the first row shows that DHSP3D does not support arbitrary topology. This is because it optimizes meshCNN and 2D XYZ map from the convex hull of the input point cloud, enforcing the output mesh to adhere to the hull’s topology. Besides, DHSP3D suffers from less realistic textures with jagged or unclear edges, since its purely self-prior property only enables it to predict point colors considering corresponding neighbors, without the ability to *dream* the unseen like our PointDreamer.

### 4.3.2 Quantitative comparisons

We summarize the quantitative results in Tables 1, and **geometry evaluation results in our supplementary file.**

TABLE 2

Anti-noise comparisons on ShapeNetCoreV2 Chairs. ‘Noisy’ means adding Gaussian noise with a standard deviation of 0.005 to the input.

| Input | Method | PSNR $\uparrow$ | SSIM $\uparrow$ | LPIPS $\downarrow$ | FID $\downarrow$ |
|-------|--------|-----------------|-----------------|--------------------|------------------|
| Noisy | SPR    | 19.64           | 0.884           | 0.170              | 65.25            |
| Noisy | NKSR   | 22.79           | 0.929           | 0.102              | 44.02            |
| Noisy | T.F.   | 26.01           | 0.944           | 0.071              | 8.21             |
| Noisy | Ours   | <b>26.26</b>    | <b>0.952</b>    | <b>0.057</b>       | <b>4.93</b>      |
| Clean | T.F.   | 26.12           | 0.947           | 0.066              | 6.83             |

TABLE 3

Performance comparison on ShapeNetCoreV2 Chairs with increased input point cloud sparsity.

| Point Number | Method | PSNR $\uparrow$ | SSIM $\uparrow$ | LPIPS $\downarrow$ | FID $\downarrow$ |
|--------------|--------|-----------------|-----------------|--------------------|------------------|
| 30k          | Ours   | <b>26.29</b>    | <b>0.9524</b>   | <b>0.057</b>       | <b>4.90</b>      |
| 25k          | Ours   | 26.28           | 0.9517          | 0.058              | 5.24             |
| 20k          | Ours   | 26.26           | 0.9509          | 0.059              | 5.70             |
| 10k          | Ours   | 26.17           | 0.9477          | 0.064              | 7.79             |
| 30k          | T.F.   | 26.12           | 0.9467          | 0.066              | 6.83             |

Our method outperforms baselines on most metrics and datasets, especially on the two perceptual metrics FID and LPIPS with a significant margin. However, regarding PSNR, which prioritizes pixel-level accuracy and thus may differ from human perception of quality, our method is sometimes outperformed by SPR. PSNR has been found to prefer blurry images [49]. We assume that SPR predicts a point’s color by *blending* nearby points’ colors, leading to blurry textures but avoiding extreme pixel-level errors. On the contrary, our method *dreams* the colors by its diffusion prior. While achieving visually better results, a few pixels with extremely high errors may lower the PSNR score.

## 4.4 Multi-view Consistency

Figure 4 (e) and our supplementary video show that, our method achieves high multi-view consistency. The reason is two-fold: (1) Unlike image-conditioned 3D generation, it’s easier to maintain multi-view consistency when reconstructing point clouds, since the input point cloud already determines the global shape and colors, leaving only local details to be *dreamed* by the model. (2) For inconsistencies in local details, our proposed Non-Border-First unprojection effectively addresses this issue; see Figure 7 (c) and Table 4.

## 4.5 Robustness against Degraded Input Quality

### 4.5.1 Anti-Noise Ability Analysis

We compare our method and baseline methods by applying them on point clouds with manually added Gaussian noise (standard deviation = 0.005) from the chair category of ShapeNetCoreV2 dataset. Table 2 shows the results, where our method, even with noisy input, outperforms baselines with clean input. Figure 5 (b) also shows our PointDreamer’s strong anti-noise ability. While baseline methods exhibit significant performance drops given noisy input, our PointDreamer’s performance degradation is minimal: even barely noticeable by human perception.

TABLE 4  
Quantitative results of replacing our NBF unprojection strategy with others. "Opt." denotes "Optimize".

| Unprojection Module | PSNR $\uparrow$ | SSIM $\uparrow$ | LPIPS $\downarrow$ | FID $\downarrow$ |
|---------------------|-----------------|-----------------|--------------------|------------------|
| Opt. Scratch        | 26.19           | 0.9473          | 0.0592             | 5.26             |
| Naive               | 26.22           | 0.9500          | 0.0587             | 5.11             |
| Opt. Naive          | 26.25           | 0.9511          | 0.0580             | 4.94             |
| NBF                 | <b>26.27</b>    | 0.9512          | 0.0579             | 5.03             |
| Opt. NBF            | 26.26           | <b>0.9516</b>   | <b>0.0574</b>      | <b>4.93</b>      |

(a) Standard input: 30k points



(b) Noisy input: 30k points + Gaussian noise (standard deviation=0.005)



(c) Sparse input: 10k points

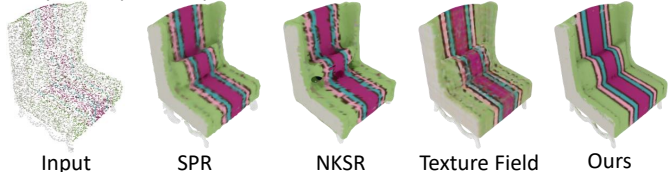


Fig. 5. Our PointDreamer’s robustness against noisy and sparse input.

#### 4.5.2 Sparsity Test

To evaluate our method’s ability to deal with sparse input, we decrease the input point number from 30k to 10k gradually, and present the results in Table 3. We can see only a small performance drop, and even with only 20k points as input, our method outperforms baseline methods with 30k points as input. When the input point number is decreased to 10k, our PointDreamer achieves higher PSNR and SSIM metrics compared to the Texture Field baseline with 30k points. We also provide visual comparisons in Figure 5 (c), where our method significantly outperforms baseline methods with only 10k points as input.

#### 4.5.3 Texture Completion Ability

Thanks to the inpainting power of the adopted 2D diffusion model, our PointDreamer has a unique ability to complete textures from incomplete scans. Figure 6 shows an example, where the point cloud of the table is incomplete since a small area is occluded by the cup during scanning. As shown in Figure 6 (a), the tablecloth is partially missing, revealing the black underside of the table below. For geometry reconstruction, such incompleteness is less challenging: both our method and baseline methods manage to fill in this hole, as shown in Figure 6 (c). If facing more challenging cases, we can also add a point cloud completion module [52] before mesh reconstruction. However, texture completion is less explored, and baseline methods cannot effectively deal with

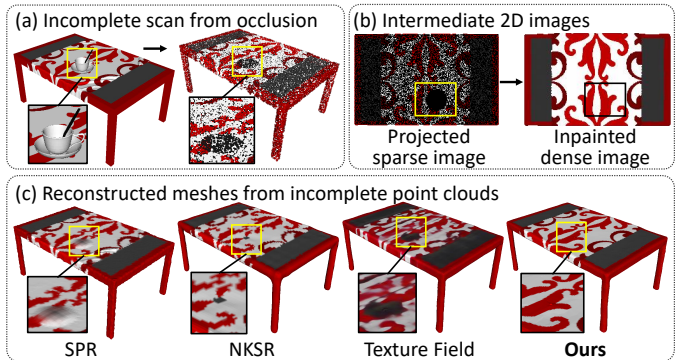


Fig. 6. Our PointDreamer’s unique completion ability. When the input point cloud is incomplete e.g. scanned from occluded objects as shown in (a), only our PointDreamer can plausibly complete the missing part with high-quality texture, as demonstrated in (c). This is benefited from the strong inpainting power of the adopted 2D diffusion model, as illustrated in (b).

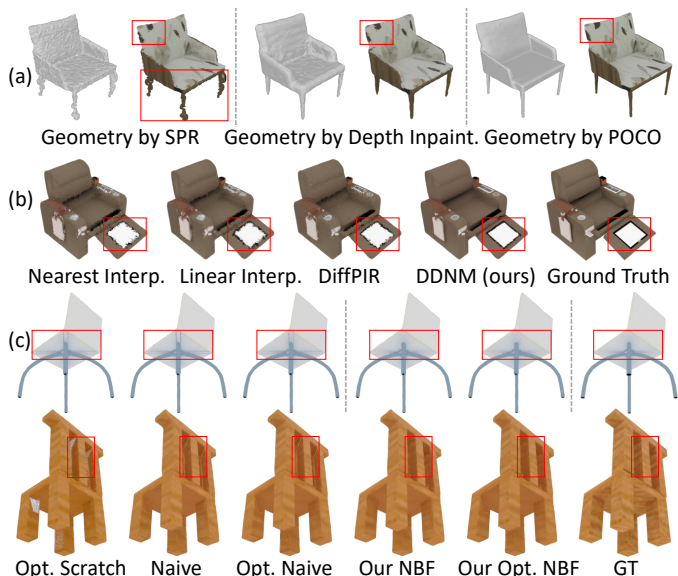


Fig. 7. Sub-Module Replacement Results: (a) Geometry module. (b) Inpainting module. (c) Unprojection module.

it. Luckily, as shown in Figure 6 (b), our diffusion-based inpainting module addresses this issue. When projecting the incomplete 3D point cloud into a 2D sparse image from the top view, the occluded part is empty to be inpainted, thanks to our hidden point removal operation. The strong diffusion prior handles this empty area well and the inpainted dense image looks plausible. As a result, as shown in Figure 6 (c), our PointDreamer completes the missing area with high-quality texture compared to other methods.

## 4.6 Method Component Analysis

We here compare different implementations for sub-modules (geometry extraction, inpainting, and unprojection module) of our method by replacing one module at a time while keeping others unchanged. All experiments in this subsection are conducted on the full test set of the chair category of ShapeNetCoreV2 dataset with Gaussian noise (standard deviation = 0.005).

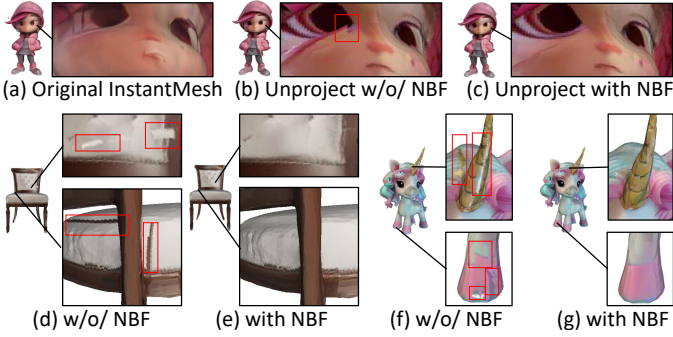


Fig. 8. Examples of adopting our proposed NBF strategy on other methods (InstantMesh [51]). (a) The original mesh generated by InstantMesh looks blurry. (b) Directly unprojecting intermediate multiview images to the mesh alleviates the blurriness, but leads to artifacts at the border of the eye as marked in a red box. (c) Using our NBF unprojection strategy avoids such artifacts. (d-g) More examples.

#### 4.6.1 Geometry Extraction

In addition to POCO, we further explore extracting geometry by SPR and depth inpainting to investigate how geometry quality influences the final reconstructed textured mesh. Please refer to our supplementary file for more details on depth inpainting and quantitative results. Figure 7 (a) shows that noisy geometry leads to noisy texture, and our adopted POCO performs the best.

#### 4.6.2 2D Inpainting

We compare different inpainting modules in our pipeline, including nearest interpolation, linear interpolation, DiffPIR [53], and our adopted DDNM, where DiffPIR is another diffusion-based 2D image restoration method with inpainting ability. We provide the visual comparisons in Figure 7 (b) and **quantitative results in our supplementary file**. As can be seen, the other three methods, though perform overall reasonably, fail to produce as clear textures as DDNM, indicating the importance of a strong inpainting module to the reconstruction performance.

#### 4.6.3 Unprojection

We present the comparison results of different unprojection strategies in Figure 7 (c) and Table 4.

- *Opt. Scratch*: optimize the texture atlas from scratch;
- *Naive*: select the best views by direction priority;
- *NBF*: select the best views by our proposed Non-Border-First strategy;
- *Opt. Naive*: further optimize *Naive*'s obtained atlas;
- *Opt. NBF*: further optimizes *NBF*'s obtained atlas while considering only loss in non-border areas.

Figure 7 (c) shows that the naive unprojection yields the above-mentioned artifacts from border areas, which can be slightly reduced by further optimization. Only our NBF and *Opt. NBF* nearly eliminate such artifacts. Table 4 also shows that our proposed NBF and *Opt. NBF* outperform other unprojection strategies.

Our NBF strategy can also work for other methods [37], [51] that reconstruct mesh textures from multiview images. For example, InstantMesh [51] reconstructs a textured 3D mesh from a single image, by first generating multiview

images, and then predicting the mesh by a large reconstruction model. As mentioned, predicting colors by a network trained with 3D data can result in blurry textures, as shown in Figure 8 (a). While unprojecting the multiview images to the mesh can achieve clearer textures, as shown in Figure 8 (b), artifacts often occur at border areas, such as the border of the eye as marked in red. Our NBF strategy effectively solved such artifacts, as shown in (c). More examples are provided in (d-g).

## 5 CONCLUSION, LIMITATIONS AND FUTURE WORK

**Conclusion.** We propose PointDreamer, a novel framework for textured mesh reconstruction from colored point cloud with SoTA performance. By utilizing diffusion-based 2D inpainting, it (1) reconstructs clear and high-quality mesh textures, addressing the common blurring issue; (2) shows high robustness against sparse, noisy, or even incomplete input, and (3) works in a zero-shot manner, requiring no extra training. We also propose a novel “Non-Border-First” strategy to unproject the colors of predicted 2D images back to 3D space. This strategy is the first to address the border-area artifact issue, which is less-explored but commonly-occurred in methods that generate 3D textures from multiview images.

**Limitations and Future Work.** (1) Like all other methods producing meshes from multi-view images, our method cannot perfectly color the small unseen areas. (2) The adopted inpainting module DDNM, though with SoTA performance, cannot perfectly inpaint all cases, especially those with extremely complex, irregular patterns or very fine details. In the future, we plan to develop an adaptive camera placement strategy to minimize invisible regions and better cover the entire mesh. Additionally, we aim to further investigate a relighting-supportive reconstruction approach: disentangling illumination effects from the input points’ colors, and reconstructing albedo colors and material information for the mesh, to better support relighting in graphics pipelines.

## REFERENCES

- [1] F. Tao, B. Xiao, Q. Qi, J. Cheng, and P. Ji, “Digital twin modeling,” *Journal of Manufacturing Systems*, vol. 64, pp. 372–389, 2022.
- [2] Y. Wang, Z. Su, N. Zhang, R. Xing, D. Liu, T. H. Luan, and X. Shen, “A survey on metaverse: Fundamentals, security, and privacy,” *IEEE Communications Surveys & Tutorials*, vol. 25, no. 1, pp. 319–352, 2022.
- [3] G. Wang, J. Zhang, F. Wang, R. Huang, and L. Fang, “Xscale-nvs: Cross-scale novel view synthesis with hash featurized manifold,” 2024.
- [4] A. Boulch and R. Marlet, “Poco: Point convolution for surface reconstruction,” in *IEEE Conference on Computer Vision and Pattern Recognition (CVPR)*, June 2022, pp. 6302–6314.
- [5] Z. Wang, S. Zhou, J. J. Park, D. Paschalidou, S. You, G. Wetzstein, L. Guibas, and A. Kadambi, “Alto: Alternating latent topologies for implicit 3d reconstruction,” in *Proceedings of the IEEE/CVF Conference on Computer Vision and Pattern Recognition (CVPR)*, June 2023, pp. 259–270.
- [6] J. Tang, J. Lei, D. Xu, F. Ma, K. Jia, and L. Zhang, “Sa-ConvOnet: Sign-agnostic optimization of convolutional occupancy networks,” in *IEEE International Conference on Computer Vision (ICCV)*, 2021, pp. 6504–6513.
- [7] M. Kazhdan and H. Hoppe, “Screened poisson surface reconstruction,” *ACM Transactions on Graphics*, vol. 32, no. 3, pp. 1–13, 2013.

- [8] X. Wei, Z. Chen, Y. Fu, Z. Cui, and Y. Zhang, "Deep hybrid self-prior for full 3d mesh generation," in *IEEE International Conference on Computer Vision (ICCV)*, October 2021, pp. 5805–5814.
- [9] J. Huang, Z. Gojic, M. Atzmon, O. Litany, S. Fidler, and F. Williams, "Neural kernel surface reconstruction," in *IEEE Conference on Computer Vision and Pattern Recognition (CVPR)*, 2023, pp. 4369–4379.
- [10] A. Gupta, W. Xiong, Y. Nie, I. Jones, and B. Oğuz, "3DGen: Triplane latent diffusion for textured mesh generation," 2023.
- [11] M. Li, Z. Zhang, S. Chen, L. Zhang, Z. Xu, X. Ren, J. Liu, and P. Sun, "Colormesh: Surface and texture reconstruction of large-scale scenes from unstructured colorful point clouds with adaptive automatic viewpoint selection," *International Journal of Applied Earth Observation and Geoinformation*, vol. 132, p. 104041, 2024. [Online]. Available: <https://www.sciencedirect.com/science/article/pii/S1569843224003959>
- [12] M. Oechsle, L. Mescheder, M. Niemeyer, T. Strauss, and A. Geiger, "Texture fields: Learning texture representations in function space," in *IEEE International Conference on Computer Vision (ICCV)*, 2019.
- [13] B. Poole, A. Jain, J. T. Barron, and B. Mildenhall, "Dreamfusion: Text-to-3d using 2d diffusion," *arXiv*, 2022.
- [14] Y. Liu, C. Lin, Z. Zeng, X. Long, L. Liu, T. Komura, and W. Wang, "Syncdreamer: Generating multiview-consistent images from a single-view image," in *International Conference on Learning Representations (ICLR)*, 2024.
- [15] C.-H. Lin, J. Gao, L. Tang, T. Takikawa, X. Zeng, X. Huang, K. Kreis, S. Fidler, M.-Y. Liu, and T.-Y. Lin, "Magic3d: High-resolution text-to-3d content creation," in *IEEE Conference on Computer Vision and Pattern Recognition (CVPR)*, 2023.
- [16] R. Chen, Y. Chen, N. Jiao, and K. Jia, "Fantasia3d: Disentangling geometry and appearance for high-quality text-to-3d content creation," in *IEEE International Conference on Computer Vision (ICCV)*, October 2023.
- [17] Z. Wang, Y. Wang, Y. Chen, C. Xiang, S. Chen, D. Yu, C. Li, H. Su, and J. Zhu, "CRM: Single image to 3D textured mesh with convolutional reconstruction model," in *European Conference on Computer Vision (ECCV)*. Springer, 2025, pp. 57–74.
- [18] J. Tang, Z. Chen, X. Chen, T. Wang, G. Zeng, and Z. Liu, "Lgm: Large multi-view gaussian model for high-resolution 3d content creation," in *European Conference on Computer Vision (ECCV)*, 2024.
- [19] J. Tang, J. Ren, H. Zhou, Z. Liu, and G. Zeng, "Dreamgaussian: Generative gaussian splatting for efficient 3d content creation," in *International Conference on Learning Representations (ICLR)*, 2024.
- [20] M. Liu, C. Xu, H. Jin, L. Chen, Z. Xu, and H. Su, "One-2-3-45: Any single image to 3d mesh in 45 seconds without per-shape optimization," *Advances in Neural Information Processing Systems*, vol. 36, 2024.
- [21] L. Melas-Kyriazi, C. Rupprecht, I. Laina, and A. Vedaldi, "Realfusion: 360 reconstruction of any object from a single image," in *IEEE Conference on Computer Vision and Pattern Recognition (CVPR)*, 2023. [Online]. Available: <https://arxiv.org/abs/2302.10663>
- [22] R. Liu, R. Wu, B. Van Hoorick, P. Tokmakov, S. Zakharov, and C. Vondrick, "Zero-1-to-3: Zero-shot one image to 3d object," in *IEEE International Conference on Computer Vision (ICCV)*, 2023, pp. 9298–9309.
- [23] J. Tang, T. Wang, B. Zhang, T. Zhang, R. Yi, L. Ma, and D. Chen, "Make-it-3d: High-fidelity 3d creation from a single image with diffusion prior," in *IEEE International Conference on Computer Vision (ICCV)*, October 2023, pp. 22 819–22 829.
- [24] Y. Wang, J. Yu, and J. Zhang, "Zero-shot image restoration using denoising diffusion null-space model," in *International Conference on Learning Representations (ICLR)*, 2022.
- [25] M. Kazhdan, M. Bolitho, and H. Hoppe, "Poisson surface reconstruction," in *Proceedings of the fourth Eurographics symposium on Geometry processing*, vol. 7, 2006, p. 0.
- [26] P. Cignoni, M. Callieri, M. Corsini, M. Dellepiane, F. Ganovelli, G. Ranzuglia et al., "Meshlab: an open-source mesh processing tool." in *Eurographics Italian chapter conference*, vol. 2008. Salerno, Italy, 2008, pp. 129–136.
- [27] Q.-Y. Zhou, J. Park, and V. Koltun, "Open3D: A modern library for 3D data processing," *arXiv:1801.09847*, 2018.
- [28] T. Shen, J. Gao, K. Yin, M.-Y. Liu, and S. Fidler, "Deep marching tetrahedra: a hybrid representation for high-resolution 3d shape synthesis," in *Advances in Neural Information Processing Systems (NeurIPS)*, 2021.
- [29] G. Qian, J. Mai, A. Hamdi, J. Ren, A. Siarohin, B. Li, H.-Y. Lee, I. Skorokhodov, P. Wonka, S. Tulyakov, and B. Ghanem, "Magic123: One image to high-quality 3d object generation using both 2d and 3d diffusion priors," in *International Conference on Learning Representations (ICLR)*, 2024.
- [30] S. Szymanowicz, C. Rupprecht, and A. Vedaldi, "Viewset diffusion: (0-)image-conditioned 3D generative models from 2D data," in *IEEE International Conference on Computer Vision (ICCV)*, 2023.
- [31] Y. Shi, P. Wang, J. Ye, L. Mai, K. Li, and X. Yang, "Mvdream: Multi-view diffusion for 3d generation," *arXiv:2308.16512*, 2023.
- [32] X. Long, Y.-C. Guo, C. Lin, Y. Liu, Z. Dou, L. Liu, Y. Ma, S.-H. Zhang, M. Habermann, C. Theobalt et al., "Wonder3d: Single image to 3d using cross-domain diffusion," in *IEEE Conference on Computer Vision and Pattern Recognition (CVPR)*, 2024.
- [33] J. Huang, J. Thies, A. Dai, A. Kundu, C. Jiang, L. J. Guibas, M. Nießner, T. Funkhouser et al., "Adversarial texture optimization from RGB-D scans," in *IEEE Conference on Computer Vision and Pattern Recognition (CVPR)*, 2020, pp. 1559–1568.
- [34] Y. Fu, Q. Yan, J. Liao, H. Zhou, J. Tang, and C. Xiao, "Seamless texture optimization for RGB-D reconstruction," *IEEE Transactions Visualization & Computer Graphics*, vol. 29, no. 3, pp. 1845–1859, 2021.
- [35] Y. Fu, Q. Yan, J. Liao, and C. Xiao, "Joint texture and geometry optimization for RGB-D reconstruction," in *IEEE Conference on Computer Vision and Pattern Recognition (CVPR)*, 2020, pp. 5950–5959.
- [36] M. Waechter, N. Moehrle, and M. Goesele, "Let there be color! Large-scale texturing of 3D reconstructions," in *European Conference on Computer Vision (ECCV)*. Springer, 2014, pp. 836–850.
- [37] K. Wu, F. Liu, Z. Cai, R. Yan, H. Wang, Y. Hu, Y. Duan, and K. Ma, "Unique3D: High-Quality and Efficient 3D Mesh Generation from a Single Image," in *International Conference on Neural Information Processing Systems (NIPS)*, 2024.
- [38] P. Dhariwal and A. Nichol, "Diffusion models beat gans on image synthesis," *Advances in neural information processing systems*, vol. 34, pp. 8780–8794, 2021.
- [39] L. Mescheder, M. Oechsle, M. Niemeyer, S. Nowozin, and A. Geiger, "Occupancy Networks: Learning 3D reconstruction in function space," in *IEEE Conference on Computer Vision and Pattern Recognition (CVPR)*, 2019, pp. 4460–4470.
- [40] S. Peng, M. Niemeyer, L. Mescheder, M. Pollefeys, and A. Geiger, "Convolutional occupancy networks," in *European Conference on Computer Vision (ECCV)*. Springer, 2020, pp. 523–540.
- [41] S. Katz, A. Tal, and R. Basri, "Direct visibility of point sets," *ACM Transactions on Graphics*, vol. 26, no. 3, p. 24–es, jul 2007. [Online]. Available: <https://doi.org/10.1145/1276377.1276407>
- [42] J. Gao, T. Shen, Z. Wang, W. Chen, K. Yin, D. Li, O. Litany, Z. Gojic, and S. Fidler, "Get3d: A generative model of high quality 3d textured shapes learned from images," in *Advances In Neural Information Processing Systems*, 2022.
- [43] J. Young, "Xatlas: Mesh parameterization / uv unwrapping library," 2022, 3. [Online]. Available: <https://github.com/jpcy/xatlas>
- [44] A. X. Chang, T. Funkhouser, L. Guibas, P. Hanrahan, Q. Huang, Z. Li, S. Savarese, M. Savva, S. Song, H. Su et al., "Shapenet: An information-rich 3d model repository," *arXiv preprint arXiv:1512.03012*, 2015.
- [45] L. Downs, A. Francis, N. Koenig, B. Kinman, R. Hickman, K. Reymann, T. B. McHugh, and V. Vanhoucke, "Google scanned objects: A high-quality dataset of 3d scanned household items," in *International Conference on Robotics and Automation (ICRA)*. IEEE, 2022, pp. 2553–2560.
- [46] T. Wu, J. Zhang, X. Fu, Y. Wang, J. Ren, L. Pan, W. Wu, L. Yang, J. Wang, C. Qian, D. Lin, and Z. Liu, "Omniobject3d: Large-vocabulary 3d object dataset for realistic perception, reconstruction and generation," in *IEEE Conference on Computer Vision and Pattern Recognition (CVPR)*, 2023.
- [47] J. Zhang, D. Ren, Z. Cai, C. K. Yeo, B. Dai, and C. C. Loy, "Monocular 3d object reconstruction with gan inversion," in *European Conference on Computer Vision (ECCV)*, 2022.
- [48] Z. Wang, A. C. Bovik, H. R. Sheikh, and E. P. Simoncelli, "Image quality assessment: from error visibility to structural similarity," *IEEE Transactions on Image Processing*, vol. 13, no. 4, pp. 600–612, 2004.
- [49] R. Zhang, P. Isola, A. A. Efros, E. Shechtman, and O. Wang, "The unreasonable effectiveness of deep features as a perceptual met-

- ric," in *IEEE Conference on Computer Vision and Pattern Recognition (CVPR)*, 2018, pp. 586–595.
- [50] M. Heusel, H. Ramsauer, T. Unterthiner, B. Nessler, and S. Hochreiter, "Gans trained by a two time-scale update rule converge to a local nash equilibrium," *Advances in neural information processing systems*, vol. 30, 2017.
- [51] J. Xu, W. Cheng, Y. Gao, X. Wang, S. Gao, and Y. Shan, "InstantMesh: Efficient 3D Mesh Generation from a Single Image with Sparse-view Large Reconstruction Models," *arXiv preprint arXiv:2404.07191*, 2024.
- [52] W. Yuan, T. Khot, D. Held, C. Mertz, and M. Hebert, "PCN: Point completion network," in *International Conference on 3D Vision (3DV)*. IEEE, 2018, pp. 728–737.
- [53] Y. Zhu, K. Zhang, J. Liang, J. Cao, B. Wen, R. Timofte, and L. V. Gool, "Denoising diffusion models for plug-and-play image restoration," in *IEEE Conference on Computer Vision and Pattern Recognition Workshops (NTIRE)*, 2023.
- [54] Griegler. (2017) Pyfusion: a python framework for volumetric depth fusion. [Online]. Available: <https://github.com/griegler/pyfusion>
- [55] M. Garland and P. S. Heckbert, "Surface simplification using quadric error metrics," in *Proceedings of the 24th Annual Conference on Computer Graphics and Interactive Techniques*, ser. SIGGRAPH '97. USA: ACM Press/Addison-Wesley Publishing Co., 1997, p. 209–216. [Online]. Available: <https://doi.org/10.1145/258734.258849>
- [56] G. Taubin, "A signal processing approach to fair surface design," in *Proceedings of the 22nd Annual Conference on Computer Graphics and Interactive Techniques*, ser. SIGGRAPH '95. New York, NY, USA: Association for Computing Machinery, 1995, p. 351–358. [Online]. Available: <https://doi.org/10.1145/218380.218473>
- [57] A. Knapitsch, J. Park, Q.-Y. Zhou, and V. Koltun, "Tanks and temples: Benchmarking large-scale scene reconstruction," *ACM Transactions on Graphics*, vol. 36, no. 4, 2017.
- [58] Y. Mao, Y. Zhang, H. Jiang, A. X. Chang, and M. Savva, "Multi-scan: Scalable rgbd scanning for 3d environments with articulated objects," in *Advances in Neural Information Processing Systems*, 2022.

## APPENDIX A GEOMETRY EVALUATION RESULTS

To compare the reconstructed geometry quality of PointDreamer and baseline methods while ignoring textures, we report geometry evaluation results in Table 5. Same as our manuscript, we use ShapeNetCoreV2 [44] (Chair, Car, Motorbike categories), Google Scanned Objects [45] and Omniobject3d [46] datasets. We follow POCO [4] to use commonly-used metrics of Chamfer L1-distance  $\times 100$  (CD), normal consistency (NC), and F-Score with threshold value 1% (FS). See POCO for more details about these metrics. Note that, as mentioned in our manuscript, we use POCO as the geometry extraction module for both our PointDreamer and the Texture Field baseline.

## APPENDIX B MORE VISUAL RESULTS

Figure 10 shows more visual comparisons of our PointDreamer against baseline methods. Figure 11 shows more visual results of our PointDreamer, including projected sparse multi-view images and inpainted dense multi-view images. We hope this can help the readers better understand our pipeline.

## APPENDIX C METHOD COMPONENT ANALYSIS

### C.1 Geometry Extraction Module Replacement Experiment

To investigate how the geometry extraction module influences the final reconstructed textured mesh, we explore three different geometry extraction methods: POCO [4] (as adopted in our manuscript), SPR [7] and depth inpainting.

#### C.1.1 Depth-Inpainting for geometry extraction

With 2D inpainting adopted as the key for our texture reconstruction, we can also introduce it to geometry reconstruction, by inpainting 2D depth maps instead of RGB images. Regarding this, we conduct experiments of depth inpainting, which refers to inpainting projected sparse 2D depth maps instead of RGB images, and then reconstructing geometry from the inpainted dense depth maps by depth fusion [54]. Specifically, we follow the following steps to reconstruct untextured meshes from input point clouds, see Figure 12:

- 1) We generate multi-view sparse depth maps by projecting 3D points to 2D, and assigning the value of each pixel as the depth value of the corresponding 3D point. Note that, similar to generating our sparse RGB images, hidden point removal is conducted for each viewpoint before projecting.
- 2) Since depth fusion requires depth maps' background pixels to have infinite values to produce a reasonable mesh, we generate foreground masks by projecting 3D points to 2D space with a relatively big point size, i.e. the number of 2D pixels occupied by each 3D point. In this way, most foreground pixels (pixels that should correspond to a point on the 3D mesh) can be occupied, and we use the

closing operation of morphology to fill the rest small holes. In addition, since we use a big point size to generate the foreground mask, the mask would be bigger than the ground truth, so we shrink the generated mask by erosion.

- 3) We inpaint the foreground pixels of the sparse depth maps into dense ones by nearest interpolation considering efficiency.
- 4) We produce an untextured mesh by depth fusion based on the inpainted dense depth maps, and conduct mesh simplification [55] and Taubin Smooth [56] to it as post-processing, to get the final untextured mesh.

#### C.1.2 Results

We present the visual comparisons in our manuscript and quantitative results in Table 6, respectively. As can be seen, POCO, as a state-of-the-art deep-learning-based surface reconstruction approach, outperforms the other two methods by a significant margin, especially regarding FID. Both SPR and Depth Inpainting suffer from noisy geometry and thus low-quality textures. This indicates that a higher-performance geometry extraction module contributes to a more refined reconstructed textured mesh.

## C.2 2D Inpainting Module Replacement Experiment

We provide the quantitative results of replacing our 2D inpainting module from DDNM [24] to nearest interpolation, linear interpolation, and DiffPIR [53] in Table 7. DiffPIR is another 2D-diffusion-based image restoration approach with inpainting ability. As can be seen, DDNM outperforms the other three methods thanks to its strong inpainting ability, which is consistent with the visual comparisons from Figure 4 (b) in our manuscript.

## APPENDIX D MORE EXPERIMENTAL RESULTS

### D.1 Effect of Different K Values (Number of Viewpoints for Projection and Inpainting)

To investigate the effect of different numbers of viewpoints (denoted as  $K$ ) for projection and inpainting, we conduct experiments on the motorbike category or ShapeNetCoreV2 dataset by using different  $K$  values including 6, 8, and 20. Table 8 shows the distribution of cameras for each setting, together with the quantitative results. We can see that more views contribute to a slightly higher reconstruction quality. Visual comparisons in Figure 13 also show that, an insufficient number of views would produce artifacts in invisible or occluded areas, thus impacting the performance.

Considering that using  $K = 20$  views is only slightly better than setting  $K = 8$ , but inpainting more views' images can be much more time-consuming, we set the number of views to be 8 for most datasets in our manuscript to balance both effectiveness and efficiency. The only exception is the motorbike category from the ShapeNetCoreV2 dataset, for which we use the 20 views instead, considering motorbikes' more complex geometry and topology.

## D.2 Impact of Degraded Input Quality: More Visual Comparisons

### D.2.1 Anti-Noise Ability Analysis

Figure 14 presents the visual comparisons of our method and baseline methods’ reconstructed meshes from noisy or clean input point clouds. Note that the reconstructed untextured meshes of noisy and clean inputs are the same, this is because our adopted POCO was trained with noisy input, so before reconstructing geometry, we manually add noise to the clean input. Overall, we have the following observations, which are consistent with the quantitative results (Table 2) in our manuscript:

- 1) As expected, all methods produce higher-quality textured meshes with clean input point clouds compared to noisy ones.
- 2) Our PointDreamer shows a relatively high anti-noise ability, where only a small performance drop is observed when giving noisy input.
- 3) Our PointDreamer with noisy input point clouds shows an even better visual effect compared to baseline methods with clean inputs.

### D.2.2 Sparsity Test

Figure 15 shows the visual comparisons of our PointDreamer’s reconstructed meshes with different numbers of points as input. There is a very small performance drop introduced by decreasing the input point number, which can sometimes be hard to notice by human eyes. This indicates a relatively high robustness of our method towards varying degrees of input sparsity.

## APPENDIX E

### IMPLEMENTATION DETAILS OF TEXTURE FIELD BASELINE

#### E.1 Network architecture

Inspired by works [10], [28] that represent 3D information by a feature tri-plane, we adopt the network architecture of the open-source Convolutional Occupancy Network [40], which also follows a tri-plane representation. Specifically, we modify its encoder from taking three-dimensional input (xyz) to six-dimensional input (xyzrgb). Then, we modify its one-dimensional output head for occupancy prediction to three-dimensional for RGB color prediction.

#### E.2 Training

We follow 3DGen [10] to train the network by the per-3D-point MSE loss on predicted and GT colors of sampled 3D points. Additionally, we also tried to employ the per-2D-pixel MSE loss of 2D images rendered from GT meshes and predicted meshes by differentiable rendering, but the experimental results are worse, as shown in Figure 16. Therefore, we adopt the per-3D-point MSE loss in our manuscript. We train the texture field network on a single NVIDIA GeForce GTX 3090 GPU with a batch size of 24 and a learning rate of 0.0001 for 2592, 024 iterations (about 356 epochs).

#### E.3 Inference.

During inference, we first use POCO [4] to predict an untextured mesh from the input point cloud, and apply UV mapping to it by Xatlas [43], which produces the 3D positions of each valid pixel in the texture atlas. We query the color of each of these 3D positions by our trained texture field network, to inpaint the texture atlas, so as to obtain the final textured mesh.

## APPENDIX F

### APPLICATIONS FOR LARGE SCENES

PointDreamer, as a zero-shot method, can be adapted to indoor or outdoor scenes. Figure 9 shows two examples from Tanks and Temples Dataset [57] and MultiScan [58] dataset. Since our adopted diffusion model only supports images at  $256 \times 256$  resolution, we downsample the scene point cloud before reconstruction. Also, our adopted POCO is relatively slow, especially with large-scale input point clouds. In the future, we may seek to develop a more large-scale-friendly version of PointDreamer, by adopting higher-resolution diffusion models and geometry reconstruction models designed for big scenes. 2D inpainting will remain our key idea, with only submodules replaced.

TABLE 5  
Geometry evaluation results of our adopted POCO and baseline methods. Note that baseline Texture Field also uses POCO for geometry extraction.

| ShapeNet Cat. | Method           | CD ↓          | NC ↑          | FS ↑          |
|---------------|------------------|---------------|---------------|---------------|
| Chair         | SPR              | 1.3094        | 0.9024        | 0.8710        |
|               | NKSR             | 0.9079        | 0.8694        | 0.8188        |
|               | POCO (TF & Ours) | <b>0.4349</b> | <b>0.9267</b> | <b>0.9632</b> |
| Car           | SPR              | 0.8428        | <b>0.8847</b> | 0.8945        |
|               | NKSR             | 0.7876        | 0.8201        | 0.8128        |
|               | POCO (TF & Ours) | <b>0.4407</b> | 0.8677        | <b>0.9462</b> |
| Motirbike     | SPR              | 4.2807        | 0.7647        | 0.6587        |
|               | NKSR             | 0.8786        | 0.6871        | 0.7249        |
|               | POCO (TF & Ours) | <b>0.4423</b> | <b>0.7663</b> | <b>0.9434</b> |
| Dataset       | Method           | CD ↓          | NC ↑          | FS ↑          |
| GSO           | SPR              | 0.8565        | 0.9446        | 0.9265        |
|               | NKSR             | 0.6149        | 0.9296        | 0.9006        |
|               | POCO (TF & Ours) | <b>0.4424</b> | <b>0.9474</b> | <b>0.9679</b> |
| OmniObject3D  | SPR              | 0.6777        | 0.9511        | 0.9407        |
|               | NKSR             | 0.6148        | 0.9424        | 0.9003        |
|               | POCO (TF & Ours) | <b>0.3393</b> | <b>0.9669</b> | <b>0.9866</b> |

TABLE 6  
Quantitative results of replacing our geometry extraction module from POCO to SPR and Depth Inpainting.

| Geometry Module  | PSNR ↑         | SSIM ↑        | LPIPS ↓       | FID ↓         |
|------------------|----------------|---------------|---------------|---------------|
| SPR              | 19.4071        | 0.8752        | 0.1777        | 74.9854       |
| Depth Inpainting | 26.2502        | 0.9466        | 0.0717        | 20.7198       |
| Our Adopted POCO | <b>26.2565</b> | <b>0.9516</b> | <b>0.0574</b> | <b>4.9326</b> |

TABLE 7  
Quantitative results of replacing our inpainting module from DDNM to nearest interpolation, linear interpolation, and DiffPIR.

| Inpainting Module     | PSNR ↑         | SSIM ↑        | LPIPS ↓       | FID ↓         |
|-----------------------|----------------|---------------|---------------|---------------|
| Nearest Interpolation | 26.1175        | 0.9457        | 0.0618        | 11.0205       |
| Linear Interpolation  | 26.1739        | 0.9474        | 0.0612        | 9.4725        |
| DiffPIR               | 26.1582        | 0.9456        | 0.0652        | 9.4823        |
| Our Adopted DDNM      | <b>26.2565</b> | <b>0.9516</b> | <b>0.0574</b> | <b>4.9326</b> |



Fig. 9. Our reconstruction results on scenes.

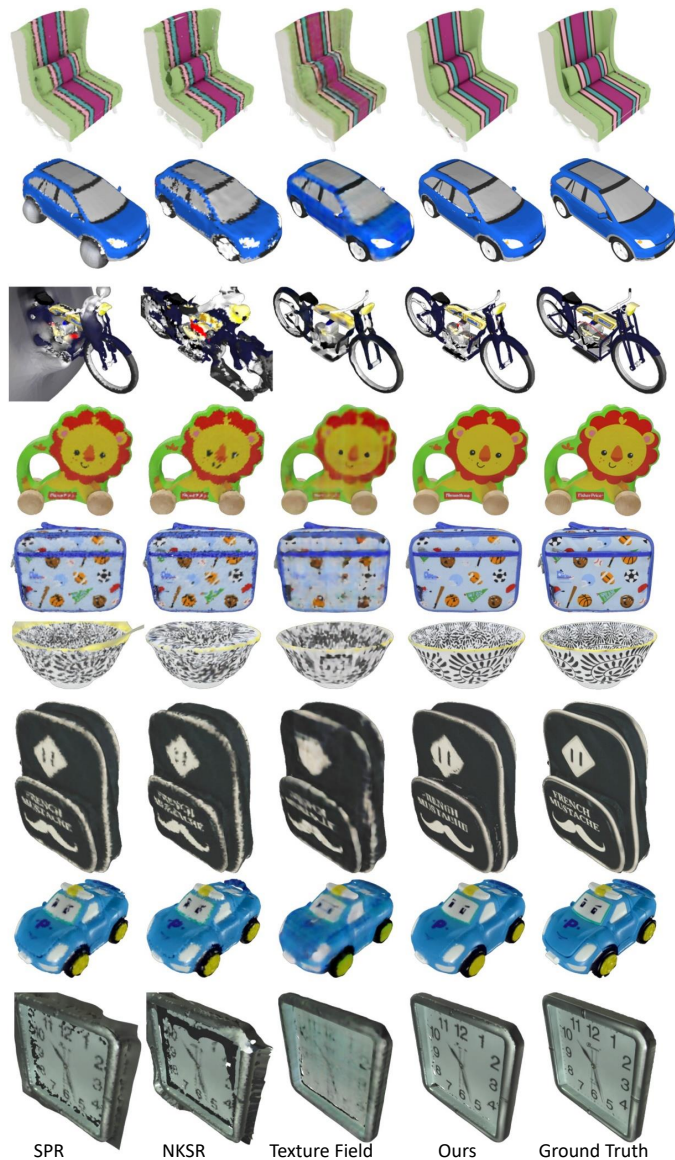


Fig. 10. More visual comparisons with baseline methods. Row 1-3: ShapeNetV2 dataset. Row 4-6: GSO dataset. Row 7-9: OmniObject3D dataset.



Fig. 11. Visual results with intermediate multi-view images.

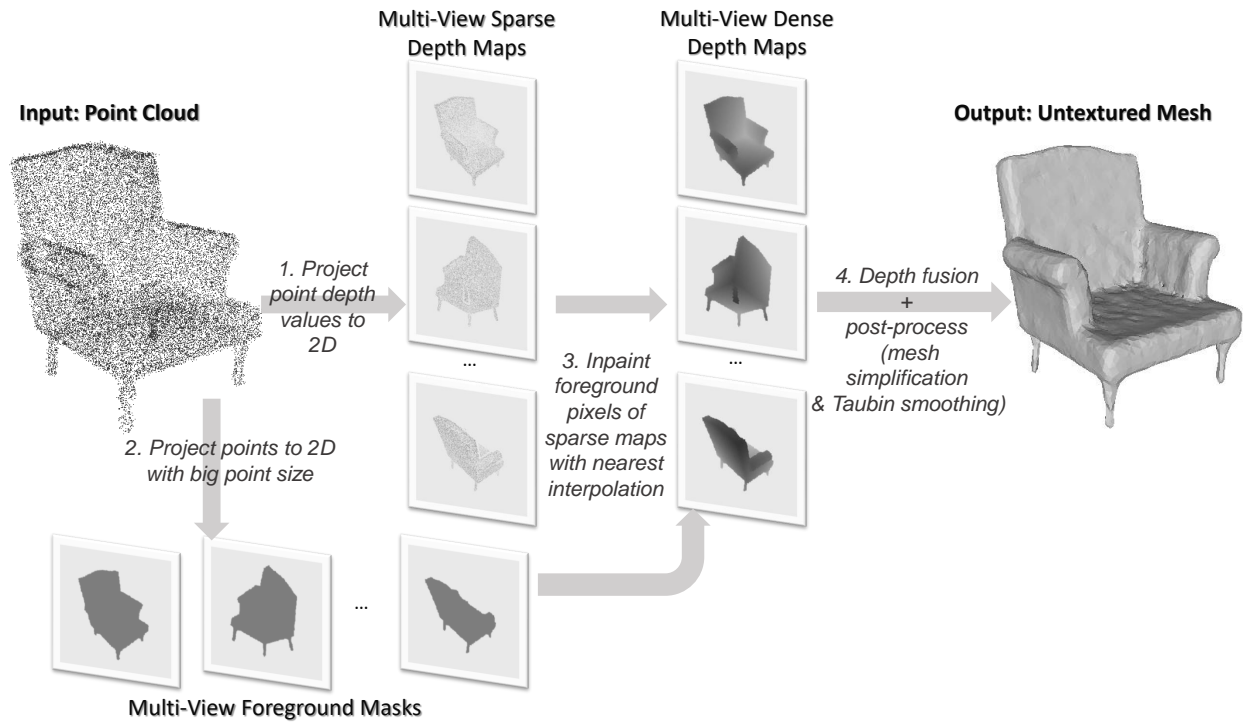


Fig. 12. Pipeline of extracting geometry by depth inpainting.

TABLE 8  
Quantitative results of using different  $K$  values (numbers of viewpoints for projection and inpainting) on the motorbike category of ShapeNetCoreV2 dataset. More views contribute to a slightly higher reconstruction quality.

| Viewpoint Number | Camera Distribution                         | PSNR $\uparrow$ | SSIM $\uparrow$ | LPIPS $\downarrow$ | FID $\downarrow$ |
|------------------|---|-----------------|-----------------|--------------------|------------------|
| 6                | At the centers of each face of a cube       | 20.8755         | 0.9273          | 0.0585             | 33.2870          |
| 8                | Evenly distributed on a Fibonacci Sphere    | 21.0664         | 0.9287          | 0.0572             | 30.2113          |
| 20               | On the 20 vertices of a regular icosahedron | <b>21.2013</b>  | <b>0.9299</b>   | <b>0.0562</b>      | <b>28.4213</b>   |

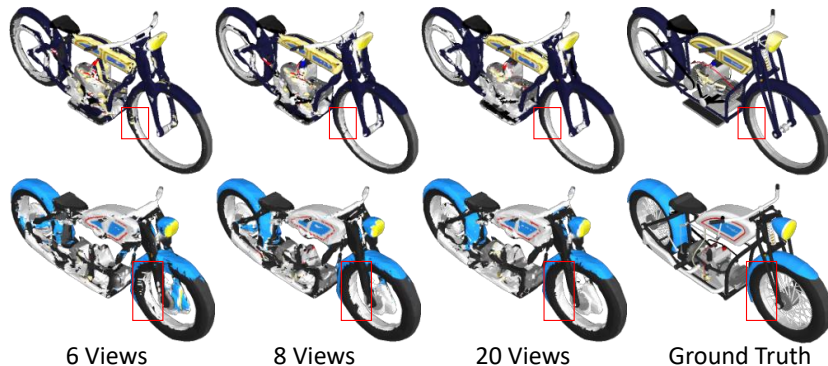


Fig. 13. Visual comparisons of our reconstructed meshes with different  $K$  values (numbers of viewpoints for projection and inpainting). An insufficient number of views would lead to artifacts in invisible or occluded areas.

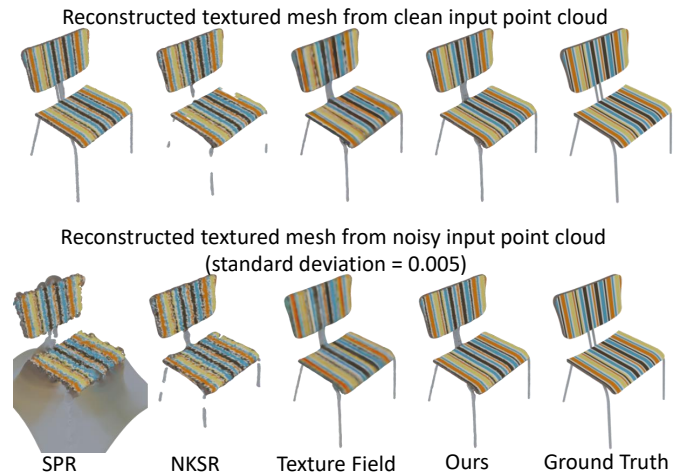
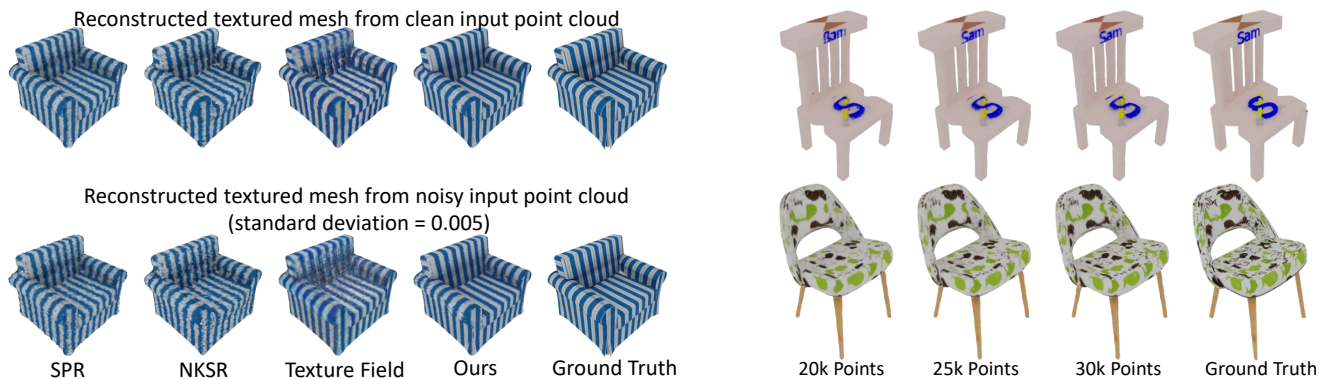


Fig. 14. Visual comparisons of our PointDreamer's and baseline methods' reconstructed meshes, with noisy or clean point clouds as input. Our PointDreamer shows a strong anti-noise ability by producing high-quality textures even with noisy input.

Fig. 15. Visual comparisons of our PointDreamer's reconstructed meshes with different numbers of points as input. There is a small performance drop when adopting sparser input, which sometimes can be hard to notice by human eyes.

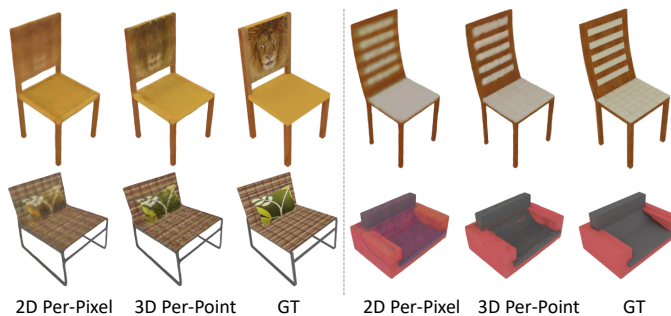


Fig. 16. Visual comparisons of the Texture Field baseline trained with different losses. "2D per-pixel" denotes rendering the generated textured mesh to multi-view 2D images, and then calculating the MSE loss between the rendered and GT images. "3D per-point" denotes calculating MSE loss between the predicted and GT colors of sampled 3D points.